Rare Met. (2025) 44(3):2094–2102
https://doi.org/10.1007/s12598-024-03024-w

RARE METALS

LETTER

Covalent organic framework assisted low-content ultrafine Ru on porous N-doped carbon for efficient hydrogen evolution reaction

Kong-Gang Qu*, Zhi-Fei Chen, Li-Hui Wang, Hai-Bo Li, Su-Yuan Zeng, Rui Li, Li-Jian Meng, Hong-Yan Chen, Qing-Xia Yao*

Received: 25 April 2024 / Revised: 15 August 2024 / Accepted: 17 August 2024 / Published online: 26 October 2024

Pt-based materials are the benchmarked catalysts in the cathodic hydrogen evolution reaction (HER) of water splitting; the prohibitive cost and scarcity of Pt immensely impede the commercialization of hydrogen energy. Ru has aroused significant concern because of its Pt-like activity and much lower price. However, it's still a top priority to minimize the Ru loading and pursue the most superior cost performance. Herein, N-rich covalent organic framework (COF) was employed to assist the preparation of ultrafine Ru, including nanoclusters and single atoms loaded onto porous N-doped carbon by a simple impregnation-pyrolysis process with a low Ru content of 6.60 wt%, exhibiting superior HER activity with mass activity of 21.86 and 11.52 $A \cdot mg^{-1}_{Ru}$ (@100 mV) in alkaline and acidic conditions, separately 14.7 and 2.12 times higher than that of commercial Pt/C. Both alkaline and acidic HERs proceed via the Volmer–Tafel route with the Tafel step as the rate-determining step (RDS), and the alkaline HER contains the water dissociation on Ru single atoms and H desorption on Ru nanoclusters accompanied by H transfer between the two. The simple synthesis, low-content Ru and exceptional activity render our catalyst greatly promising as an alternative to commercial Pt/C in the advancement of hydrogen economy.

The overconsumption of fossil fuels arouses mounting anxiety about the global energy dilemma and the greenhouse effect. Hydrogen, as an energy vector, can be greenly converted from renewable electricity by water splitting and is an ideal substitute for carbon-based fuels [1, 2]. Nowadays, noble-metal Pt-based electrocatalysts are identified as the most powerful catalysts for hydrogen evolution reaction (HER) [3]. However, the inherent drawbacks of Pt, such as high cost and rare sources, seriously restrict its scalable application [4, 5]. The development of low-price catalysts is thus important to advance the sustainable hydrogen generation. Due to the similar binding energy between Ru–H and Pt–H and the fact that Ru costs only 1/3 of Pt metal [6], Ru-based electrocatalysts have alternatively been considered the most viable contenders for Pt-based catalysts [7–11]. Nonetheless, to further improve the cost performance of noble-metal Ru-based catalysts, the atom utilization efficiency of Ru should be maximized [12–14], which necessitates the high dispersity of metal in combination with a large specific surface area, assuring the adequate exposure of the active sites and thus the high apparent performance [15, 16].

Recently, covalent organic frameworks (COFs) have prevailed as a unique type of functional material with multiple merits, including tailored pore structure, highly accessible surface area and versatile heteroatoms [17]. Thereinto, Schiff-base chemistry-based N-rich COFs have been profusely explored due to the abundant molecular

Supplementary Information The online version contains supplementary material available at https://doi.org/10.1007/s12598-024-03024-w.

K.-G. Qu*, Z.-F. Chen, L.-H. Wang, H.-B. Li, S.-Y. Zeng, R. Li, H.-Y. Chen, Q.-X. Yao*
School of Chemistry and Chemical Engineering, Shandong Provincial Key Laboratory/Collaborative Innovation Center of Chemical Energy Storage and Novel Cell Technology, Liaocheng University, Liaocheng 252059, China
e-mail: qukonggang@lcu.edu.cn

Q.-X. Yao
e-mail: yaoqingxia@lcu.edu.cn

L.-J. Meng
Centre of Innovation in Engineering and Industrial Technology, Instituto Superior de Engenharia do Porto, Instituto Politecnico do Porto, 4249-015 Porto, Portugal

precursors, uncomplicated experimental conditions and enhanced stability [18]. In this case, the N-rich COFs could robustly anchor metals through abundant N heteroatoms for the high dispersity of metal and also furnish high porosity to expose metal sites, thus highly promising to effectively improve atom utilization efficiency. Additionally, pyrolysis-free COFs have been directly employed as electrocatalysts or supports for electrocatalytic applications, but with the average performance [19–22], primarily limited by the intrinsically undistinguished electrical conductivity of COFs. Thus, thermal annealing is still one valid approach to substantially enhance the conductivity and the catalytic activity of COFs-based materials [23–25].

The imine-linked COFs have been widely studied and show satisfactory performance in adsorption, catalysis, energy storage, etc. [18]. Herein, we employed an imine-linked stomatal N-rich COF to effectively absorb Ru^{3+} through the direct impregnation method, which consequently produced ultrafine Ru species embedded in COF-derived nitrogen-doped carbons (Ru/NC) after pyrolysis. The robust confinement of N-rich COF can facilitate the formation of ultrafine Ru with low content of 6.60 wt%, including 1.3-nm nanoclusters and single atoms together with large surface area, rich pores and abundant N dopants, thus collectively resulting in excellent alkaline and acidic HER activity, with mass activity of 21.86 and 11.52 $A{\cdot}mg^{-1}_{Ru}$ (@100 mV), 14.7 and 2.12 times higher than that of commercial Pt/C, respectively. The in-depth experiments reveal the synergistic mechanism in alkaline HER involving the water dissociation on Ru single atoms and the generated hydrogen transfer onto Ru nanoclusters accompanied by the subsequent H desorption. This work not only provides a promising strategy for a highly cost-effective Ru-based HER electrocatalyst but also promotes the advancement of COF-based materials in practical applications.

The preparative routes of N-rich COF and Ru/NC are illustrated in Fig. S1 and Scheme 1 [26, 27]. Fourier transform infrared spectroscopy (FTIR) spectra were firstly measured as shown in Fig. S2a; the signal intensity of the aldehyde groups from tri-(4-formacylphenoxy)-1,3,5-triazine (TFPTA) and NH_2 group from 2,4,6-trihydrazino-1,3,5-triazine (THTA) separately centered at 1701 and 3312 cm^{-1} is significantly lowered, implying the successful formation of COF [26]. Additionally, X-ray diffractometer (XRD) pattern of N-rich COF shows two distinct peaks at 3.4° and 6.0° (Fig. S2b), which confirms the presence of a highly ordered hexagonal structure, also consistent with the reported result previously [26]. After the introduction of Ru^{3+}, followed by high-temperature pyrolysis, the COFs were carbonized into an N-doped carbon (NC) loaded with Ru. The morphology and structure of Ru/NC were first characterized by scanning electron microscopy (SEM) and transmission electron microscopy (TEM). SEM image reveals the two-dimensional lamellar morphology with the size of a dozen micrometers of Ru/NC (Fig. S3). The images of high-angle annular dark-field scanning TEM (HAADF-STEM) show the honeycomb-like carbon structure loaded with ultrafine Ru nanoclusters with a mean diameter of only 1.3 nm (Fig. 1a, b) and the lattice fringe of 0.214 nm correlates well to the (002) plane of Ru with a hexagonal close-packed crystal structure (Fig. 1c). Meanwhile, the single atoms of Ru can also be observed which are abundantly dispersed around Ru nanoclusters (Fig. 1c). The formation of ultrasmall Ru species can be attributed to the robust confinement of N-rich COF [28]. The images of TEM elemental mapping prove that the N, O and Ru elements are evenly distributed on Ru/NC (Fig. 1d). As the control samples, COF-derived NC shows the flake morphology with homogeneous distribution of N and O dopants (Fig. S4), while for Ru nanoparticles on carbon black (Ru/C), the small Ru particles of several

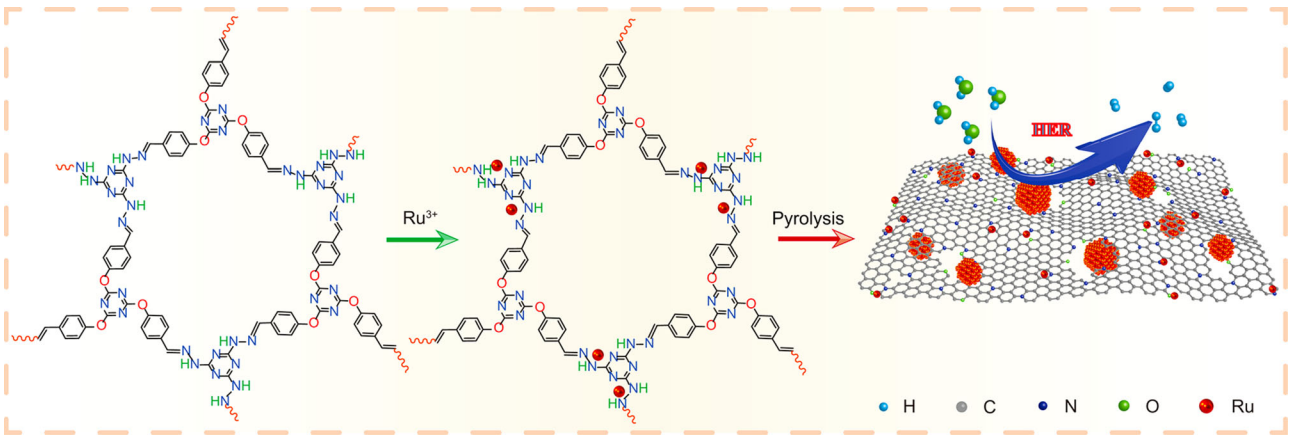

Scheme 1 Schematic illustration of synthesis of Ru/NC

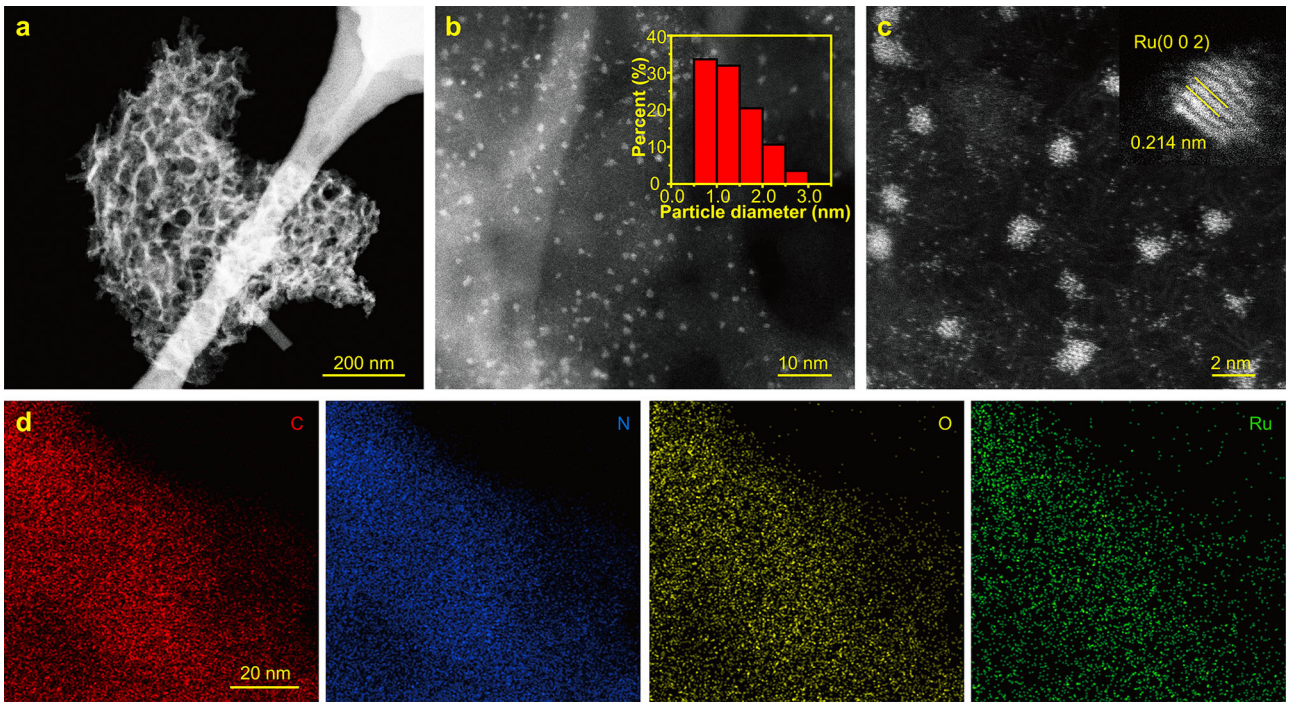

Fig. 1 **a–c** HAADF-TEM images of Ru/NC at different magnifications with size distribution histogram (inset in **b**); **d** TEM elemental mappings of Ru/NC catalyst

nanometres were loaded on the sphere surfaces of carbon black (Fig. S5) [29].

Furthermore, the textural properties of the obtained materials were examined by the N_2 adsorption–desorption isotherms. As depicted in Fig. 2a, the isotherms of type IV for NC and Ru/NC indicate the presence of mesopores; the surface areas of NC and Ru/NC can reach up to 485.6 and 496.9 $m^2 \cdot g^{-1}$ together with the average pore sizes of 5.95 and 5.26 nm, respectively, proving the excellent surface properties obviously derived from N-rich COF [30, 31], which would be greatly beneficial in the catalytical applications. Additionally, Raman spectra reveal the D band at 1350 cm^{-1} and G band at 1590 cm^{-1} (Fig. 2b), suggesting the existence of both graphitic carbon and extrinsic defects, and the intensity ratio of D band and G band (I_D/I_G) of Ru/NC (0.87) was somewhat lower than that of NC (0.90), implying a high degree of graphitization due to the presence of metal Ru, which would provide the favorable electroconductivity for electrocatalysis [30, 32]. Powder X-ray diffraction (PXRD) of samples was also measured, as shown in Fig. 2c. The patterns of the three samples all show similar broad diffraction peaks at 23.8° and 43.1°, associated with graphitic carbon [33]. None of the samples shows diffraction peaks of elemental or oxidic Ru species, suggesting the absence of larger Ru species, in line with the prior TEM analyses [34].

Surface X-ray photoelectron spectroscopy (XPS) was performed to examine the chemical components of samples. The survey scan (Fig. 2d) shows the existence of Ru (1.18 at%), C (81.51 at%), N (6.7 at%) and O (6.39 at%) on the surface of Ru/NC (Table S1). Firstly, in the Ru 3p spectra of Ru/NC (Fig. 2e), it is clear that the peak at the binding energy centered at 461.6 and 484.0 eV matching with $3p_{3/2}$ and $3p_{1/2}$ of Ru°, while the signals at 464.8 and 487.2 eV belong to the $3p_{3/2}$ and $3p_{1/2}$ of Ru^{n+} probably originated from Ru–N and Ru–O bonds [35, 36]. Noteworthily, the Ru° peak of Ru/NC has a shift of about 0.42 eV to lower energy than Ru/C, demonstrating an electron donation from N to Ru [36]. Additionally, the fitting four peaks of N 1s spectra (Fig. 2f) separately correspond to graphitic N (400.6 eV), pyrrolic N (399.9 eV), Ru–N (399.2 eV) and pyridinic N (397.7 eV) species [37, 38]. Collectively, XPS analyses verify the abundant N dopants in Ru/NC together with the formation of Ru–N bonds, arising from the strong metal-support interaction between N-doped carbon and Ru species, including Ru nanoclusters and single atoms, which can modulate the electronic property of Ru and thus improve the electrocatalytic activity [39]. For O 1s spectra (Fig. S6), the peaks centered at 529.3, 530.3, 532.1 and 534.3 eV are associated with Ru–O, C=O, C–O–C and adsorbed O species, respectively [40]. The presence of O can endow the catalyst with benign hydrophilicity, thus facilitating the electrode/electrolyte interfacial contact and gas evolution. Furthermore, the inductively coupled plasma optical emission spectrometry (ICP-OES) result manifests the content of Ru in Ru/NC is only 6.60 wt%.

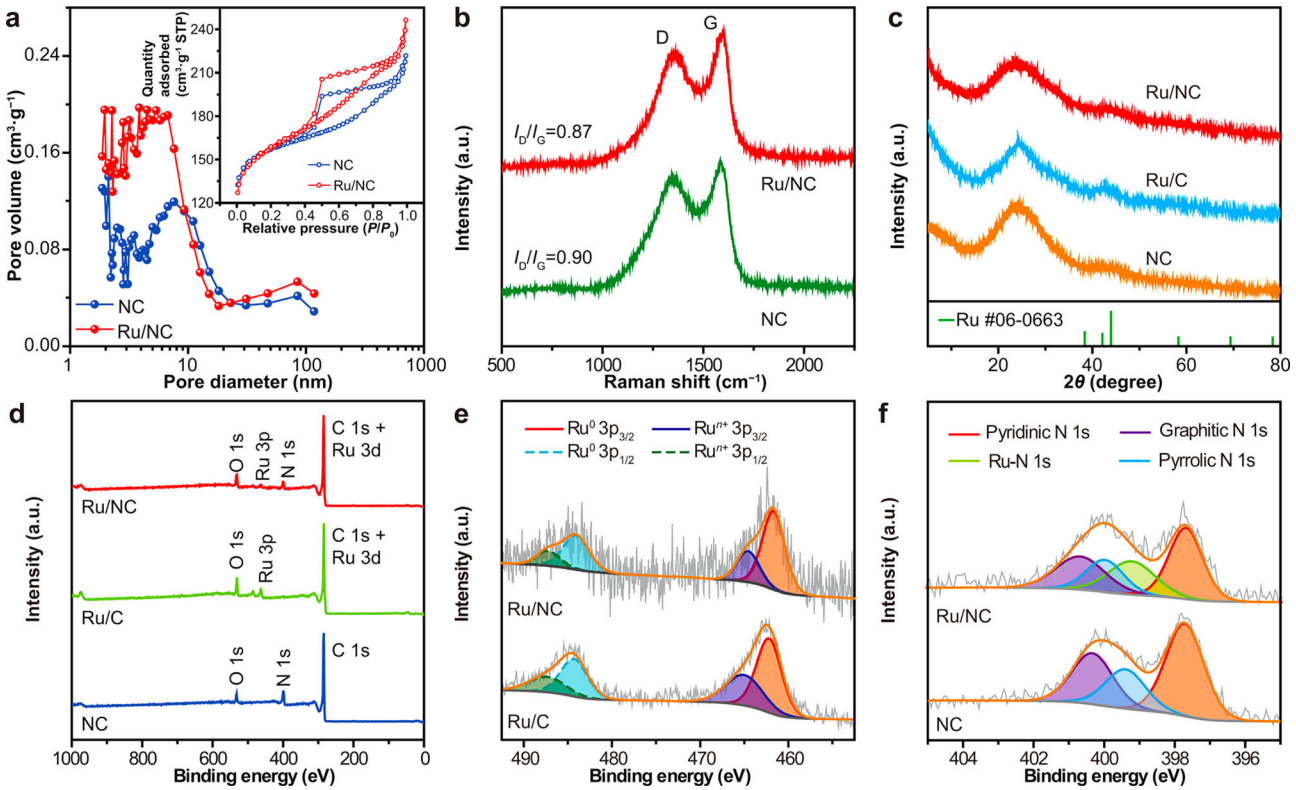

Fig. 2 **a** Pore size distribution plot and (inset) N_2 adsorption–desorption isotherm and **b** Raman spectrum of Ru/NC and NC; **c** XRD patterns and **d** XPS survey spectra of Ru/NC, Ru/C and NC, respectively; **e** Ru 3p XPS spectra of Ru/NC and Ru/C; **f** N 1s XPS spectra of Ru/NC and NC

The HER activity of Ru/NC was first investigated in a 1.0 M KOH electrolyte. Prominently, the linear scan voltammetry (LSV) curves show that Ru/NC only demands an ultrasmall potential of 10.0 mV to reach 10 $mA{\cdot}cm^{-2}$, the lowest value among different samples, while the overpotentials for the other samples were substantially higher. Moreover, the Ru/NC catalyst demonstrates exceptional performance at large current density, and only needs a low overpotentials of 70.2 mV to achieve 100 $mA{\cdot}cm^{-2}$, significantly lower than those of Ru/C (161.8 mV) and commercial Pt/C (146.7 mV) (Fig. 3a). Meanwhile, Ru/NC shows a Tafel slope of 33.9 $mV{\cdot}dec^{-1}$ (Fig. 3b), much smaller than those of Pt/C (63.2 $mV{\cdot}dec^{-1}$) and Ru/C (65.3 $mV{\cdot}dec^{-1}$). As known, the HER mechanism involves the Volmer-Heyrovsky or Volmer-Tafel pathway. The possible pathway and rate-determining step (RDS) can be simply discerned from the Tafel slope, considering the Volmer, Heyrovsky and Tafel reactions have theoretical Tafel slope values of 120, 40 and 30 $mV{\cdot}dec^{-1}$, respectively [41]. Therefore, the Volmer-Tafel route occurs on Ru/NC with the Tafel step as the RDS, while the Volmer-Heyrovsky route on Pt/C with the water dissociation as the RDS. Additionally, an ultralow charge-transfer resistance (R_{ct}) of 1.11 Ω was observed on Ru/NC (Fig. 3c), suggesting the greatly beneficial HER kinetics.

The underpotential deposition of copper (Cu-UPD) was then measured to determine the electrochemical surface area (ECSA) and the number of active sites (n) of samples (Fig. S7 and Table S2) [42–44]. Specifically, Ru/NC has the largest ECSA of 247.0 $m^2{\cdot}g^{-1}_{Ru}$, in comparison to commercial Pt/C (48.43 $m^2{\cdot}g^{-1}_{Pt}$) and Ru/C (30.02 $m^2{\cdot}g^{-1}_{Ru}$) [45]. Thus, the calculated turnover frequency (TOF) value of Ru/NC is 20.66 $H_2{\cdot}s^{-1}$ at 100 mV (Fig. 3d), much higher than those of Pt/C (7.22 $H_2{\cdot}s^{-1}$) and Ru/C (8.89 $H_2{\cdot}s^{-1}$). Moreover, Ru/NC demonstrates an exceptional mass activity of 21.86 $A{\cdot}mg^{-1}_{Ru}$ at the overpotential of 100 mV (Fig. 3e), surpassing that of Ru/C (1.14 $A{\cdot}mg^{-1}_{Ru}$ @ 100 mV) and commercial Pt/C (1.49 $A{\cdot}mg^{-1}_{Pt}$ @ 100 mV) by 19.2 and 14.7 times, respectively. Obviously, Ru/NC shows an outstanding intrinsic activity for alkaline HER, greatly exceeding Pt/C.

For the acidic HER, Fig. 3f reveals a small overpotential of 41.8 mV at 10 $mA{\cdot}cm^{-2}$ on Ru/NC, matchable with that of Pt/C (43.6 mV) and better than that of Ru/C (50.1 mV). Additionally, the Tafel slope of Ru/NC (29.3 $mV{\cdot}dec^{-1}$, Fig. 3g) is close to that of Pt/C (27.5 $mV{\cdot}dec^{-1}$) and lower than that of Ru/C (43.6 $mV{\cdot}dec^{-1}$), explaining the same Volmer-Tafel mechanism on Ru/NC and Pt/C [44, 46]. Ru/NC exhibits a smaller R_{ct} value of 1.95 Ω (Fig. 3h) than those of Pt/C (0.44 Ω) and Ru/C (4.22 Ω), suggesting the

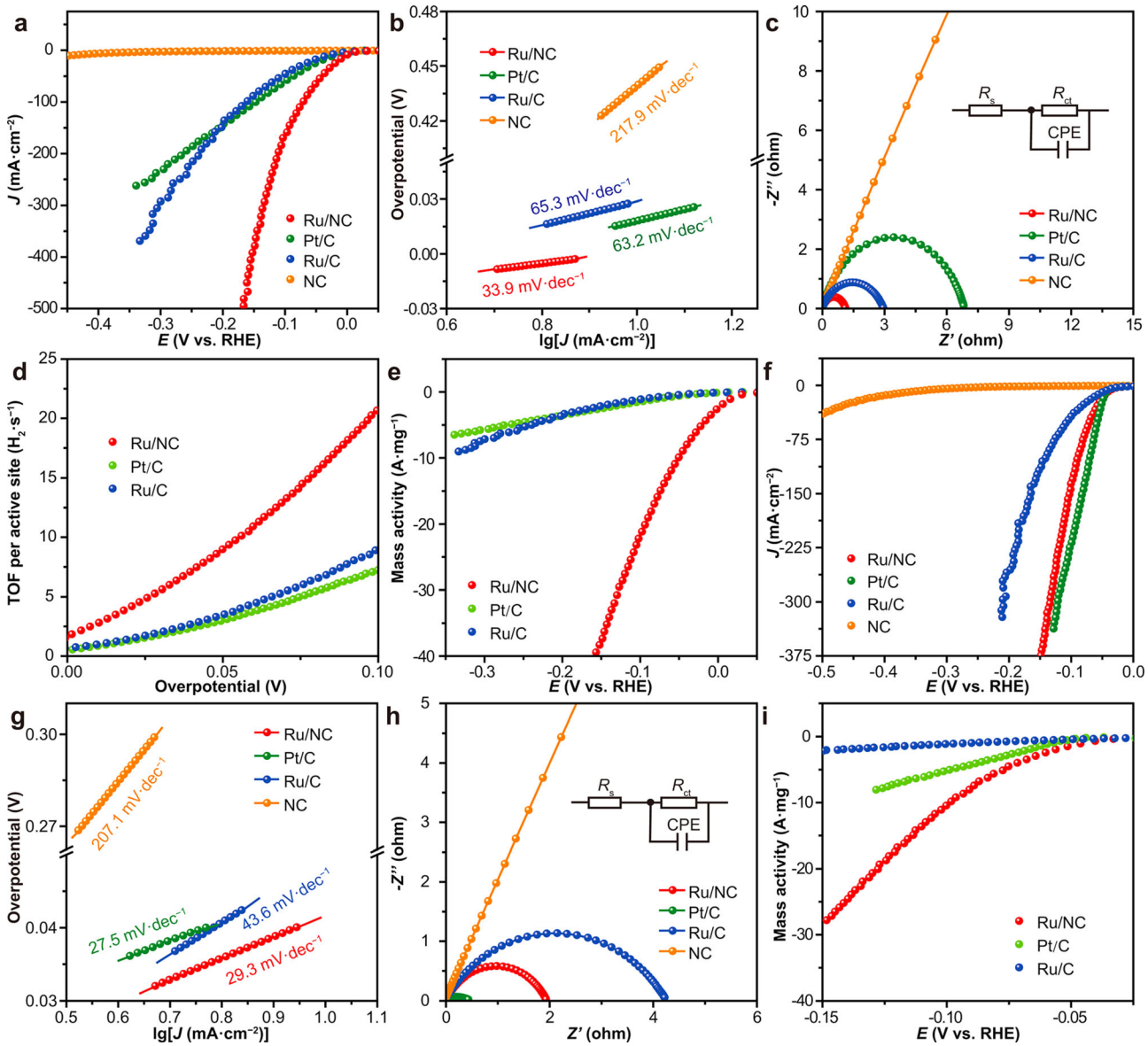

Fig. 3 **a** HER LSV curves in 1.0 M KOH; **b** corresponding HER Tafel slopes; **c** EIS of HER in 1.0 M KOH; **d** calculated TOF and **e** calculated mass activity values for alkaline HER on Ru/NC, Pt/C and Ru/C; **f** HER LSV curves in 0.5 M H_2SO_4; **g** corresponding HER Tafel slopes; **h** EIS of HER in 0.5 M H_2SO_4; **i** calculated mass activity values for acidic HER on Ru/NC, Pt/C and Ru/C

efficient HER kinetics at the interface of Ru/NC and the electrolyte. Furthermore, in an acidic environment, the calculated TOF value of Ru/NC is 10.02 $H_2{\cdot}s^{-1}$@100 mV (Fig. S8), inferior to that of Pt/C (26.68 $H_2{\cdot}s^{-1}$) and better than that of Ru/C (9.02 $H_2{\cdot}s^{-1}$). However, Ru/NC can achieve a mass activity of 11.52 $A{\cdot}mg^{-1}_{Ru}$ at the overpotential of 100 mV (Fig. 3i), much better than those of Pt/C (5.44 $A{\cdot}mg^{-1}_{Pt}$) and Ru/C (1.11 $A{\cdot}mg^{-1}_{Ru}$). Moreover, the LSV curves after successive 3000 cyclic voltammetry (CV) cycles show only a very small degradation, and the current density also remains almost constant in the continuous 30 h's chronoamperometric test under both alkaline and acidic conditions (Figs. S9, S10). The samples collected after stability tests in two electrolytes retain the original microstructure as well. Additionally, Fig. S11 manifests nearly 100% Faradaic efficiency on Ru/NC with almost identical hydrogen production rate to the theoretical value for alkaline and acidic HER. Therefore, Ru/NC has a large advantage over Pt/C for both alkaline and acidic HER with regard to its excellent apparent activity, robust stability and low Ru content.

The alkaline HER includes the initial water dissociation and subsequent H absorption/desorption, which was thus put emphasis on discussing here. To further understand the origin of electrocatalytic activity from two types of Ru sites, the poison test was conducted with $EDTA^{2-}$ and

SCN^-. It is recognized that $EDTA^{2-}$ can passivate single-atom metal, while SCN^- can block all the metal sites [47]. Figures 4a, S12a reveal that the addition of $EDTA^{2-}$ can only lead to a small loss of activity, while SCN^- can suppress the most part of activity. For example, the overpotential at 100 $mA{\cdot}cm^{-2}$ only has a small increase from 70.2 to 99.5 mV with $EDTA^{2-}$, but sharply rises to 276 mV with SCN^-, manifesting Ru nanoclusters play more important roles than single-atom Ru. In addition, based on the Tafel slope analyses, the alkaline HER of Ru/NC obeys the Volmer–Tafel route with the Tafel step, i.e., H desorption, as the RDS. Consequently, H desorption very likely occurs on Ru nanoclusters.

Furthermore, the kinetic isotope effect (KIE) experiment was conducted in 1.0 M KOH/D_2O electrolyte to obtain insight into the role of hydrogen transfer during the alkaline HER [48, 49]. The KIE values were extracted through the current density ratios from H_2O and D_2O electrolytes (J_H/J_D), and if the KIE value is larger than 1.5, the presence of hydrogen transfer can be evidenced. As shown in Figs. 4b, S12b, at the current density of 200, 300, 400 and 500 $mA{\cdot}cm^{-2}$ for J_H, the needed overpotentials are 110.0, 134.4, 150.7 and 169.6 mV, respectively. At the aforesaid overpotentials, the values of J_D are 50.9, 71.9, 89.1 and 108.7 $mA{\cdot}cm^{-2}$, respectively, which are quite lower. Accordingly, the calculated KIEs values range from 3.93 to 4.60 (larger than 1.5), manifesting the hydrogen transfer takes place during the alkaline HER process. Therefore, the possible routes of alkaline HER on Ru/NC may consist of the water dissociation on Ru single atoms, and the hydrogen transfer from Ru single atoms to Ru nanoclusters, and H desorption on Ru nanoclusters (Fig. 4c), which is also accordant with the previous reports [35, 45, 50, 51].

The superior electrocatalytic performance of Ru/NC may benefit from the manifold advantages of COF. Firstly, the employed COF owns a large number of N heteroatoms, which can strongly anchor metals and thus facilitate the formation of ultrafine Ru clusters and single atoms, endowing the maximized atom utilization efficiency of noble metal Ru [17]. Secondly, the formed Ru–N bonds between Ru species and carbon substrate not only can stabilize the Ru species but more importantly, can regulate the electronic structure of Ru active sites, therefore enhancing the unit activity [7, 45]. Thirdly, the derived doped carbon inherits the large surface area and abundant pores from COF, ensuring full exposure of active sites as well as smooth mass transfer during HER [52].

In summary, by taking advantage of one N-rich COF, ultrafine Ru, including 1.3-nm nanoclusters and single atoms embedded into porous N-doped carbon, was simply synthesized as a high-efficiency and durable electrocatalyst for alkaline and acidic HER, with much better mass activity than commercial Pt/C. The abundant heteroatoms, Ru–N metal-substrate interaction and large surface area with rich pores can collectively endow low-content Ru (6.60 wt%) with superior HER performance. Further

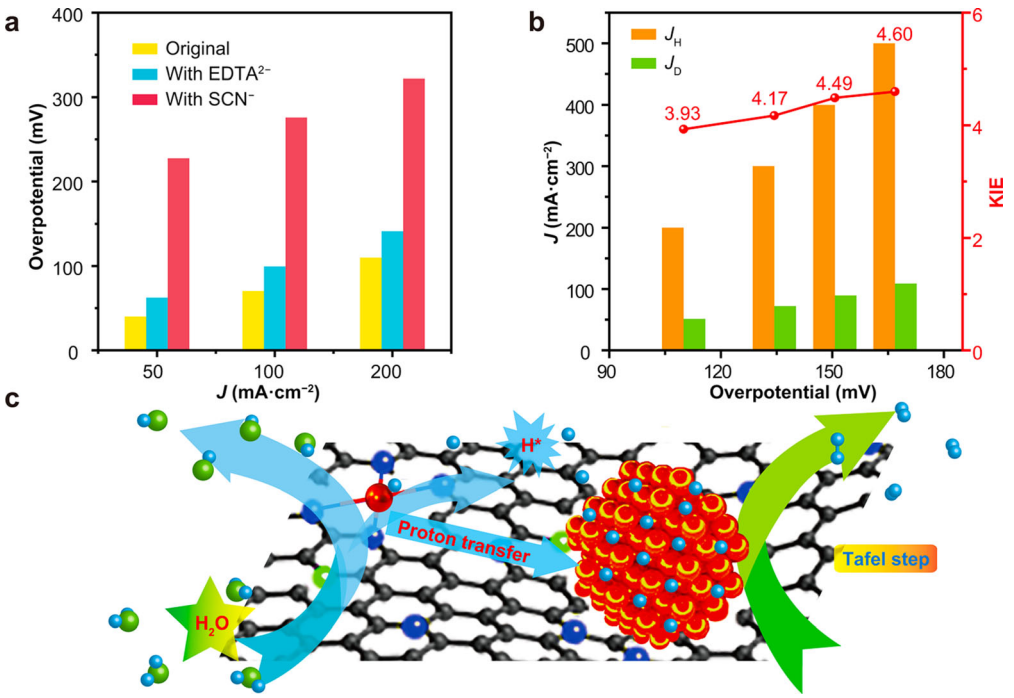

Fig. 4 **a** Required overpotentials of Ru/NC at a certain current density with and without SCN^- and $EDTA^{2-}$ for alkaline HER; **b** calculated KIE values from J_H/J_D at different potentials on Ru/NC; **c** corresponding mechanism of alkaline HER on Ru/NC

experiments verify Ru single atoms and nanoclusters separately responsible for water dissociation and H desorption accompanied by H transfer between the two. The combination of the simple preparation method, the ultralow content of Ru and the absence of template agents make the newly prepared catalyst highly cost-effective and thus great potential for commercialization.

Acknowledgements This work was financially supported by the Development Project of Youth Innovation Team in Shandong Colleges and Universities (No. 2019KJC031), the Natural Science Foundation of Shandong Province (Nos. ZR2019MB064, ZR2021MB122 and ZR2022MB137) and the Doctoral Program of Liaocheng University (No. 318051608).

Declarations

Conflict of interests The authors declare that they have no conflict of interest.

References

[1] Wang LF, Yang RX, Fu JZ, Cao YY, Ding RF, Xu XH. Vertically aligned W(Mo)S_2/N-W(Mo)C-based light-assisted electrocatalysis for hydrogen evolution in acidic solutions. Rare Met. 2023;42(5):1535. https://doi.org/10.1007/s12598-022-02250-4.

[2] Chen MN, Lin ZJ, Ren Y, Wang X, Li M, Sun DM, Tang YW, Fu GT. Universal synthesis of rare earth-doped FeP nanorod arrays for the hydrogen evolution reaction. Mater Chem Front. 2023;7(18):4132. https://doi.org/10.1039/D3QM00516J.

[3] Yu DH, Zuo C, Gao Y, Zhou SP, Lu J, Liu F. Research progress on electrolysis of hydrogen-deposited noble metal electrocatalysts. Chin J Rare Met. 2023;47(11):1573. https://doi.org/10.13373/j.cnki.cjrm.XY19120030.

[4] Deng X, Zheng XD, Gong ZW, Tan WY, Pei XD. Research progress on single metal atom catalysts for hydrogen production by PEM water electrolysis with lower costs. Chin J Rare Met. 2023;47(01):43. https://doi.org/10.13373/j.cnki.cjrm.XY22060014.

[5] Lin ZP, Wang ZP, Gong JJ, Jin TC, Shen SJ, Zhang QH, Wang JC, Zhong WW. Reversed spillover effect activated by Pt atom dimers boosts alkaline hydrogen evolution reaction. Adv Funct Mater. 2023;33(45):2307510. https://doi.org/10.1002/adfm.202307510.

[6] Ma XF, Xiao H, Jing YY, Gao Y, He YL, Zhao M, Jia JF, Wu HS. Site difference influence of anchored Ru in mesoporous carbon on electrocatalytic performance toward pH-universal hydrogen evolution reaction. Rare Met. 2023;42(12):4015. https://doi.org/10.1007/s12598-023-02389-8.

[7] Zhong G, Zhao R, Shi YR, Li CR, He L, He L, Huang Y. Thermal shock synthesis of carbon nanotubes supporting small-sized rhenium nanoparticles for efficient electrocatalytic hydrogen evolution. Rare Met. 2023;42(7):2166. https://doi.org/10.1007/s12598-022-02259-9.

[8] Sajjad S, Wang C, Deng CW, Ji F, Ali T, Shezad B, Ji HQ, Yan CL. Unravelling critical role of metal cation engineering in boosting hydrogen evolution reaction activity of molybdenum diselenide. Rare Met. 2022;41(6):1851. https://doi.org/10.1007/s12598-021-01948-1.

[9] Wang ZP, Lin ZP, Wang YL, Shen SJ, Zhang QH, Wang JC, Zhong WW. Nontrivial topological surface states in Ru_3Sn_7 toward wide pH-range hydrogen evolution reaction. Adv Mater. 2023;35(25):2302007. https://doi.org/10.1002/adma.202302007.

[10] Tang RR, Yang Y, Zhou YT, Yu XY. Rational Design of heterostructured Ru cluster-based catalyst for pH universal hydrogen evolution reaction and high-performance Zn-H_2O battery. Adv Funct Mater. 2024;34(5):2301925. https://doi.org/10.1002/adfm.202301925.

[11] Wei YW, Yang G, Xu XX, Liu YY, Kang NX, Li BJ, Wang YZ, Zhao YX. Ultrafine Ru nanoparticles anchored on core–shell structured zeolite-carbon for efficient catalysis of hydrogen generation. Rare Met. 2023;42(7):2324. https://doi.org/10.1007/s12598-022-02246-0.

[12] Shen SJ, Zhang HH, Song K, Wang ZP, Shang TT, Gao A, Zhang QH, Gu L, Zhong WW. Multi-d electron synergy in $LaNi_{1-x}Co_xRu$ intermetallics boosts electrocatalytic hydrogen evolution. Angew Chem Int Ed. 2024;63(1):e202315340. https://doi.org/10.1002/anie.202315340.

[13] Yan P, Yang T, Lin MX, Guo YN, Qi ZP, Luo QQ, Yu XY. "One stone five birds" plasma activation strategy synergistic with Ru single atoms doping boosting the hydrogen evolution performance of metal hydroxide. Adv Funct Mater. 2023;33(25):2301343. https://doi.org/10.1002/adfm.202301343.

[14] Saira Y, Li ZJ, Zhu Y, Liu QC, Luo WK, Wang Y, Gong MX, Fu GT, Tang YW. Low-loaded Ru on hollow SnO_2 for enhanced electrocatalytic hydrogen evolution. Chem Commun. 2024;60(20):2768. https://doi.org/10.1039/D3CC06209K.

[15] Zhou F, Zhou Y, Liu GG, Wang CT, Wang J. Recent advances in nanostructured electrocatalysts for hydrogen evolution reaction. Rare Met. 2021;40(12):3375. https://doi.org/10.1007/s12598-021-01735-y.

[16] Chen J, Ha Y, Wang RR, Liu YX, Xu HB, Shang B, Wu RB, Pan HG. Inner Co Synergizing outer Ru supported on carbon nanotubes for efficient pH-universal hydrogen evolution catalysis. Nano-Micro Lett. 2022;14(1):186. https://doi.org/10.1007/s40820-022-00933-2.

[17] Huang LJ, Yang J, Asakura Y, Shuai Q, Yamauchi Y. Nanoarchitectonics of hollow covalent organic frameworks: synthesis and applications. ACS Nano. 2023;17(10):8918. https://doi.org/10.1021/acsnano.3c01758.

[18] Yuan YY, Xi XX, Bao T, Bian PG, Pei F, Zhang XH, Wang SF, Wen W. Integrating bimetallic nanoparticles with covalent organic frameworks as multifunctional nanozyme for colorimetric detection of hydrogen peroxide and glutathione. J Anal Test. 2024;8(3):278. https://doi.org/10.1007/s41664-024-00298-y.

[19] Wang AJ, Cheng LX, Zhao W, Shen XL, Zhu WH. Electrochemical hydrogen and oxygen evolution reactions from a cobalt-porphyrin-based covalent organic polymer. J Colloid Interface Sci. 2020;579:598. https://doi.org/10.1016/j.jcis.2020.06.109.

[20] Guo JN, Lin CY, Xia ZH, Xiang ZH. A pyrolysis-free covalent organic polymer for oxygen reduction. Angew Chem Int Ed. 2018;57(38):12567. https://doi.org/10.1002/anie.201808226.

[21] Liu ZY, Lin YD, Hao Y, Chen HN, Guo ZW, Li XX, Zheng ST. Recent advances in polyoxoniobate-catalyzed reactions. Tungsten. 2022;4(2):81. https://doi.org/10.1007/s42864-021-00134-1.

[22] Zhao YX, Liang Y, Wu DX, Tian H, Xia T, Wang WX, Xie WY, Hu XM, Tian XL, Chen Q. Ruthenium complex of sp^2 carbon-conjugated covalent organic frameworks as an efficient electrocatalyst for hydrogen evolution. Small. 2022;18(14):2107750. https://doi.org/10.1002/smll.202107750.

[23] Seo JM, Noh HJ, Jeon JP, Kim H, Han GF, Kwak SK, Jeong HY, Wang LL, Li F, Baek JB. Conductive and ultrastable covalent organic framework/carbon hybrid as an ideal electrocatalytic platform. J Am Chem Soc. 2022;144(43):19973. https://doi.org/10.1021/jacs.2c08344.

[24] Zhao HH, Zhang XH, Zhang YW, Song YZ, Li C, Liu K, Ma DX. Covalent organic framework-derived CoRu nanoalloy doped macro–microporous carbon for efficient electrocatalysis. J Mater Chem A. 2022;10(47):25272. https://doi.org/10.1039/D2TA08224A.
[25] Long JJ, Wu HC, Liu YT, Ding YY, Yao QL, Metin O, Lu ZH. Hydrogen production from chemical hydrogen storage materials over copper-based catalysts. cMat. 2024;1(1):e10. https://doi.org/10.1002/cmt2.10.
[26] Dinari M, Hatami M. Novel N-riched crystalline covalent organic framework as a highly porous adsorbent for effective cadmium removal. J Environ Chem Eng. 2019;7(1):102907. https://doi.org/10.1016/j.jece.2019.102907.
[27] Zhao YJ, Sun Y, Li HB, Zeng SY, Li R, Yao QX, Chen HY, Zheng Y, Qu KG. Highly enhanced hydrazine oxidation on bifunctional Ni tailored by alloying for energy-efficient hydrogen production. J Colloid Interface Sci. 2023;652:1848. https://doi.org/10.1016/j.jcis.2023.09.003.
[28] Wang X, Chen WX, Zhang L, Yao T, Liu W, Lin Y, Ju HX, Dong JC, Zheng LR, Yan WS, Zheng XS, Li ZJ, Wang XQ, Yang J, He DS, Wang Y, Deng ZX, Wu YE, Li YD. Uncoordinated amine groups of metal–organic frameworks to anchor single Ru sites as chemoselective catalysts toward the hydrogenation of quinoline. J Am Chem Soc. 2017;139(28):9419. https://doi.org/10.1021/jacs.7b01686.
[29] Chen CQ, Fan XS, Zhou C, Lin L, Luo Y, Au CT, Cai GH, Wang XY, Jiang LL. Hydrogen production from ammonia decomposition over Ni/CeO_2 catalyst: effect of CeO_2 morphology. J Rare Earths. 2023;41(7):1014. https://doi.org/10.1016/j.jre.2022.05.001.
[30] Yan BL, Liu DP, Feng XL, Shao MZ, Zhang Y. Ru species supported on MOF-derived N-doped TiO_2/C hybrids as efficient electrocatalytic/photocatalytic hydrogen evolution reaction catalysts. Adv Funct Mater. 2020;30(31):2003007. https://doi.org/10.1002/adfm.202003007.
[31] Zhang W, Guo XM, Li C, Xue JY, Xu WY, Niu Z, Gu HW, Redshaw C, Lang JP. Ultralong nitrogen/sulfur Co-doped carbon nano-hollow-sphere chains with encapsulated cobalt nanoparticles for highly efficient oxygen electrocatalysis. Carbon Energy. 2023;5(8): e317. https://doi.org/10.1002/cey2.317.
[32] Shi LY, Bai WC, Deng Y, Sun JF, Zhang SF. Modification of Cu-based electrocatalysts and their research progress for electrochemical hydrogen evolution reaction. Copper Eng. 2023;6:51. https://doi.org/10.3969/j.issn.1009-3842.2023.06.006.
[33] Ai J, Zhang XL, Bai T, Shen Q, Oleynikov P, Duan YY, Terasaki O, Che SA, Han L. Synchronous quantitative analysis of chiral mesostructured inorganic crystals by 3D electron diffraction tomography. Nat Commun. 2022;13(1):5718. https://doi.org/10.1038/s41467-022-33443-1.
[34] Shao XD, Liang MF, Kumar A, Liu XH, Jin HY, Ajmal S, Bui VQ, Bui HTD, Lee JS, Tran NQ, Yu JM, Cho YH, Kim MG, Lee HY. Amorphization of metal nanoparticles by 2D twisted polymer for super hydrogen evolution reaction. Adv Energy Mater. 2022;12(16):2102257. https://doi.org/10.1002/aenm.202102257.
[35] Chen JL, Liao XL, Chen S, Lu TT, Sun XT, Cao LX, Wang H. Self–supported CuBi bimetal nanodendrites for CO_2 electrochemical reduction. Copper Eng. 2023;(1):1. https://doi.org/10.3969/j.issn.1009-3842.2023.01.001.
[36] Xu S, Niu M, Zhao GW, Ming SJ, Li XY, Zhu QL, Ding LX, Kim MJ, Alothman AA, Mushab MSS, Yamauchi Y. Size control and electronic manipulation of Ru catalyst over B, N co-doped carbon network for high-performance hydrogen evolution reaction. Nano Res. 2023;16(5):6212. https://doi.org/10.1007/s12274-022-5250-1.
[37] Liu QR, Tian H, Dai ZH, Sun HQ, Liu J, Ao ZM, Wang SB, Han C, Liu SM. Nitrogen-doped carbon nanospheres-modified graphitic carbon nitride with outstanding photocatalytic activity. Nano-Micro Lett. 2020;12(1):24. https://doi.org/10.1007/s40820-019-0358-x.
[38] Zhang Y, Wang WY, Wang YP, Zhang YF. ZnS encapsulated in N/S co–doped carbon fiber as a composite material for Li storage. Copper Eng. 2023;(4):23. https://doi.org/10.3969/j.issn.1009–3842.2023.04.003.
[39] Chen ZF, Wang LH, Li HB, Zeng SY, Li R, Chen HY, Zheng Y, Yao QX, Qu KG. Highly enhanced bifunctionality by trace Co doping into Ru matrix towards hydrazine oxidation-assisted energy-saving hydrogen production. Fuel. 2024;360:130602. https://doi.org/10.1016/j.fuel.2023.130602.
[40] Ge RX, Li L, Su JW, Lin YC, Tian ZQ, Chen L. Ultrafine defective RuO_2 electrocatayst integrated on carbon cloth for robust water oxidation in acidic media. Adv Energy Mater. 2019;9(35):1901313. https://doi.org/10.1002/aenm.201901313.
[41] Ye SH, Luo FY, Xu TT, Zhang PY, Shi HD, Qin SQ, Wu JP, He CX, Ouyang XP, Zhang QL, Liu JH, Sun XL. Boosting the alkaline hydrogen evolution of Ru nanoclusters anchored on B/N-doped graphene by accelerating water dissociation. Nano Energy. 2020;68:104301. https://doi.org/10.1016/j.nanoen.2019.104301.
[42] Li H, Chang SH, Zhang MM. Research progress on properties tuning and products of Cu–based catalyst in electrocatalytic CO_2 reduction. Copper Eng. 2023;(6):38. https://doi.org/10.3969/j.issn.1009–3842.2023.06.005.
[43] He HY, Song WL. Microstructure and mechanical property of Cu–contained high–entropy alloys. Copper Eng. 2023;(2):34. https://doi.org/10.3969/j.issn.1009–3842.2023.02.005.
[44] Kweon DH, Okyay MS, Kim SJ, Jeon JP, Noh HJ, Park NJ, Mahmood J, Baek JB. Ruthenium anchored on carbon nanotube electrocatalyst for hydrogen production with enhanced Faradaic efficiency. Nat Commun. 2020;11(1):1278. https://doi.org/10.1038/s41467-020-15069-3.
[45] Guan XY, Wu QN, Li HB, Zeng SY, Yao QX, Li R, Chen HY, Zheng Y, Qu KG. Identifying the roles of Ru single atoms and nanoclusters for energy-efficient hydrogen production assisted by electrocatalytic hydrazine oxidation. Appl Catal B Environ. 2023;323:122145. https://doi.org/10.1016/j.apcatb.2022.122145.
[46] Tang BY, Bisbey RP, Lodaya KM, Toh WL, Surendranath Y. Reaction environment impacts charge transfer but not chemical reaction steps in hydrogen evolution catalysis. Nat Catal. 2023;6(4):339. https://doi.org/10.1038/s41929-023-00943-2.
[47] Fan XL, Liu C, Wu MY, Gao BX, Zheng LY, Zhang YH, Zhang HB, Gao QS, Cao XM, Tang Y. Synergistic effect of dual active sites over Ru/α-MoC for accelerating alkaline hydrogen evolution reaction. Appl Catal B Environ. 2022;318:121867. https://doi.org/10.1016/j.apcatb.2022.121867.
[48] Fu HQ, Zhou M, Liu PF, Liu PR, Yin HJ, Sun KZ, Yang HG, Al-Mamun M, Hu PJ, Wang HF, Zhao HJ. Hydrogen spillover-bridged Volmer/Tafel processes enabling ampere-level current density alkaline hydrogen evolution reaction under low overpotential. J Am Chem Soc. 2022;144(13):6028. https://doi.org/10.1021/jacs.2c01094.
[49] Dai J, Zhu YL, Chen Y, Wen X, Long MC, Wu XH, Hu ZW, Guan DQ, Wang XX, Zhou C, Lin Q, Sun YF, Weng SC, Wang HT, Zhou W, Shao ZP. Hydrogen spillover in complex oxide multifunctional sites improves acidic hydrogen evolution electrocatalysis. Nat Commun. 2022;13(1):1189. https://doi.org/10.1038/s41467-022-28843-2.
[50] Yang CD, Wu ZH, Zhao ZY, Gao Y, Ma T, He C, Wu CZ, Liu XK, Luo XL, Li S, Cheng C, Zhao CS. Electronic structure-dependent water-dissociation pathways of ruthenium-based

catalysts in alkaline H_2-evolution. Small. 2023;19(14):2206949. https://doi.org/10.1002/smll.202206949.

[51] Zhu YP, Fan K, Hsu CS, Chen G, Chen CS, Liu TC, Lin ZZ, She SX, Li LQ, Zhou HM, Zhu Y, Chen HM, Huang HT. Supported ruthenium single-atom and clustered catalysts outperform benchmark Pt for alkaline hydrogen evolution. Adv Mater. 2023;35(35):2301133. https://doi.org/10.1002/adma.202301133.

[52] Guan XY, Sun Y, Zhao SM, Li HB, Zeng SY, Yao QX, Li R, Chen HY, Qu KG. Selectively nucleotide-derived RuP on N, P-codoped carbon with engineered mesopores for energy-efficient hydrogen production assisted by hydrazine oxidation. SusMat. 2024;4(1):166. https://doi.org/10.1002/sus2.186.